Microstructural, Tribological, and Degradation Properties of Al$_2$O$_3$- and CeO$_2$-Doped 3 mol.% Yttria-Stabilized Zirconia Bioceramic for Biomedical Applications

Mohsen Golieskardi, Meenaloshini Satgunam, Dinesh Ragurajan, Md Enamul Hoque, and Angela Min Hwei Ng

Among the ceramic materials available for load-bearing bioimplant applications, yttria-stabilized zirconia (Y-TZP) holds great potential owing to its superior mechanical properties (e.g., fracture toughness $\sim$ 4.5 MPam$^{1/2}$). However, the degradation concern of Y-TZP over long exposure to body fluids limits its applications. To overcome this limitation, the current work focuses on developing stabilized zirconia ceramics doped with Al$_2$O$_3$ and CeO$_2$ through an easily available low-cost sintering technique. The microstructural, tribological, and degradation properties of Al$_2$O$_3$- and CeO$_2$-doped 3Y-TZP bioceramic were investigated. The volumetric wear and roughness values of Al$_2$O$_3$- and CeO$_2$-doped 3Y-TZP samples were found to be much lower compared to undoped 3Y-TZP samples. Relative densities of above 97.5% of the theoretical densities ($>$ 6.1 g/cm^{-3}) were obtained in 3Y-TZP sintered at 1450 °C. Low-temperature degradation resistance was observed when immersing the samples in Ringer's solution at 37 °C over a period of 24 weeks. The weight loss and SEM images of the samples were analyzed to generate the samples' degradation patterns. The results indicate that the incorporation of dopants is technically beneficial in terms of ceramic sample aging.

1. Introduction

Biomaterials are synthetic materials with the potential of being used to replace damaged body tissues. They can be applied to make prostheses of body organs for instance, which serve different purposes, for example, constructing rehabilitation devices, organ implants, organ augmentations, etc. As for developments in the implantology field, several materials have been invented to improve the quality of prostheses that are applied for either fixing or replacing body tissues. Since most of the biomaterials used for this purpose are ceramics, metals, and polymers, spectacular improvements have been made in many cases, such as bone reconstruction and replacement joints or teeth. Every group has its own shortcomings and benefits. In the case of ceramics, it has been reckoned to possess the most excellent biocompatibility property that comes with biostable, bioactive, and bioresorbable attributes. As for the disadvantages, ceramics has issues with fragility and hardness. As such, the yttria-stabilized tetragonal zirconia polycrystal (Y-TZP) refers to ceramic with advanced engineering to enhance its hardness property (Ref [1], [2]). This is because the toughening mechanism results in crack suppression and expansion of volume (Ref [3]). This mechanism can result in much higher strength and toughness than in most of the other monolithic ceramics and approaching the strength and toughness of low-strength metals (Ref [4-6]). Upon firing, this Y-TZP ceramic gets a single-phase tetragonal structure of fine grains ($<$ 0.5 μm). This fine-grained single-phase tetragonal structure provides excellent strength ($>$ 700 MPa) (Ref [7], [8]), high toughness ($>$ 4.5 MPam$^{1/2}$) (Ref [9]), and good wear resistance (Ref [10]) that makes it ideal for a number of structural applications. Besides, Guazzato et al. (Ref [11]) asserted that this toughening attribute makes the Y-TZP a suitable material for hip and dental implants. Furthermore, the element of zirconia promotes fixation at the surrounding tissues without any leaching or bonding in a biological manner, upon implantation.

Nevertheless, despite its supreme properties, the Y-TZP ceramic has a major drawback in terms of aging in the presence of liquid/moisture which is known as hydrothermal aging or low-temperature degradation (LTD) (Ref [12-14]). This occurrence of degradation is followed by failure of mechanical property due to the conversion from tetragonal (t) to monoclinic (m) due to aging, thus the primary reason for the failure of ball and zirconia artificial joint head (Ref [15]).

The aim of this work is to investigate the effect of adding Al$_2$O$_3$ and CeO$_2$ to 3Y-TZP ceramic on obtaining enhanced wear resistance and low friction for hip prostheses. The enhanced effect of this ceramic's mechanical and microstructural properties and its aging behavior in an autoclave and Ringer's solution is also examined.

Mohsen Golieskardi, Meenaloshini Satgunam, and **Dinesh Ragurajan**, Department of Mechanical Engineering, Faculty of Engineering, Universiti Tenaga Nasional, Kajang, Selangor, Malaysia; **Md Enamul Hoque**, Department of Biomedical Engineering, Military Institute of Science and Technology (MIST), Dhaka, Bangladesh; and **Angela Min Hwei Ng**, Tissue Engineering Center, Universiti Kebangsaan Malaysia Medical Center, Kuala Lumpur, Malaysia. Contact e-mail: mohsen_golieskardi@yahoo.com.

2. Experimental Procedures

2.1 Processing

The ceramic compositions investigated in this study include 3 mol.% of yttria-stabilized zirconia powder (code KZ-3YF) manufactured by Kyoritsu Ltd., Japan, as the base powder, and cerium oxide (CeO_2) and aluminum oxide (Al_2O_3) manufactured by Sigma-Aldrich as dopants. The starting powders were mixed using a wet-milling method with zirconia balls as mixing medium and ethanol as another mixing medium to break the agglomerates and further reduce the particle size. Based on Taguchi method, nine different compositions of Al_2O_3- and CeO_2-doped 3Y-TZP were prepared through a novel process involving ultrasonification and wet milling as shown in Table 1. This was followed by cold uniaxial pressing into pellets of 10 mm diameter using a hydraulic press. All the Al_2O_3- and CeO_2-doped 3Y-TZP powder mixtures were sintered in atmospheric condition at a ramp rate of 10 °C/min, temperatures ranging from 1250 to 1550 °C, and holding time of 2 h before cooling to room temperature.

2.2 Microstructural and Mechanical Characterizations

X-ray diffraction (XRD) provided data for identification through gem cross sections of the materials, thus portraying the crystalline stages present. The stage examination of 3Y-TZP was done with XRD, utilizing low-plot $(111)c$, t, $(111)m$ and $(111)m$ reflections to facilitate the quantitative determination of the monoclinic stage substance evident in the material. This strategy was utilized to discover the stages exhibited in the powders and sintered ceramic surfaces, and to screen the advancement of the aging-impelled (t)-to-(m) phase transformation (Ref 16). A Rigaku diffractometer was used with Cu-Kα radiation operating at 35 kV/15 mA in step mode with a 0.02° 2θ step and a step scan of 0.5°/min over the 2θ range of 27°-36° that covers the (m) and $(t) + (c)$ related (111) peaks. Although the (c)- and (t)-ZrO$_2$ could be resolved at this stage, the (m)-ZrO$_2$ fraction may still be obtained. The microstructural characterization for various sintering temperatures and compositions was investigated using a Philips XL30 scanning electron microscope (SEM). Prior to SEM analysis, the samples were polished to a 6-μm finish and subsequently coated with platinum. The grain size of the elements present in the material was determined from the scanning electron micrographs using the average grain intercept method.

Table 1 Composition of base material and dopants powder

Composition	3Y-TZP, wt.%	Al_2O_3, wt.%	CeO_2, wt.%
1	99.00	0.70	0.30
2	99.20	0.50	0.30
3	99.40	0.30	0.30
4	98.80	0.70	0.50
5	99.00	0.50	0.50
6	99.20	0.30	0.50
7	98.60	0.70	0.70
8	98.80	0.50	0.70
9	99.00	0.30	0.70

The Archimedes method was employed to measure the density of sintered samples by using distilled water as the medium for immersion via electronic balance, which is retrofitted by using a kit that measures density (Mettler Toledo, Switzerland). Next, the Young's modulus (E) had been identified via sonic resonance for samples in rectangular shape via a testing tool obtained commercially (GrindoSonic: MK5 'Industrial,' Belgium). Such a tool allows identifying the frequency of resonance for a sample through monitoring evaluation the vibrational harmonics of the sample, in which tapping induces vibrations from the samples. Besides, this Young's modulus had been determined empirically via the frequency of resonance (ASTM E1876-97). Furthermore, the 3Y-TZP flexural strength had been identified via transverse bending test (3-point method) by adhering to ASTM—C1161-13 procedures.

2.3 Tribological Property Investigation

On top of that, a friction test had been conducted via pin-on-disk tester. The tribometer (TR 283 Series, Ducom, Bangalore, India), which had been deemed apt for frequencies that are low, had been applied to simulate contact pressure, temperature, and speed in hip joints. This particular simulating machine is designed particularly to model the contact of the sliding line of a planar interface with cylindrical. For example, in order to simulate the walking speed of human at 10 mm/s, 2 mm stroke length and 5 Hz frequency are set. Next, the Ringer solution had been applied as a lubricant, while 37 °C was set as the temperature of the human body. Moreover, three varied disks of surface profiles with two compositions ($0.3Al_2O_3/0.3CeO_2$ and $0.3Al_2O_3/0.5CeO_2$) had been examined. Besides, the pin had been connected to a metallic holder and fixed to hinder rotation on its own. Three static load sets (10, 30 and 50 N) were applied, which were equivalent to 216.6, 375.2, and 484.4 MPa of Hertz pressure, to the $0.3Al_2O_3/0.3CeO_2$ interfaces and 220.8, 382.5, and 493.8 MPa of Hertz pressure to the $0.3Al_2O_3/0.5CeO_2$ interfaces. The three contact pressures refer to normal weight, overweight, and obese patients.

2.4 Material Degradation Investigation

In order to examine the aging behavior of both undoped and Al_2O_3- and CeO_2-doped 3Y-TZP, the disk samples of each composition were subjected to autoclave conditions for up to 100 h. Initially, two samples were placed into an acid digestion bomb (Parr Instruments, USA) followed by 20 mL of distilled water. The bomb was then placed in an oven and held at 134 °C to convert the water into superheated steam at 1 bar vapor pressure. During the test, the samples were taken out at selected intervals and the aging-induced (t)-to-(m) phase transformation was monitored by XRD technique.

The resorption rate of the 3Y-TZP samples was studied in Ringer's solution at 37 °C to simulate the human body conditions. Ten disks of each sample category were placed in a 24-well cell culture dish plate. Five hundred microliters of Ringer's solution (B. Braun, USA) were added to each well containing one disk, fully immersing the disk. The plate was placed in a CO_2 incubator set at 37 °C. An appropriate volume of Ringer's solution was added every 2 days in order to maintain the initial volume. Upon removing the disks from the wells with a blunt forceps, excess solution was allowed to drip off the disks before placing them on a weighing boat. The disks

were weighed using a digital laboratory analytical weighing machine (Sartorius, USA; resolution 0.0001 g).

2.5 Modeling Summary

The variation of flexural strength, young's modulus, and surface roughness for 3Y-TZP with different amounts of Al_2O_3 and CeO_2 as shown in Table 1 sintered at temperatures between 1250 and 1450 °C was performed. Using the response surface methodology (RSM) method, in specific Design Expert software as statistical tool, input variables (weight percentage of Al_2O_3, weight percentage of CeO_2, and sintering temperature) with respect to Young's modulus, flexural strength, and surface roughness were optimized. RSM was able to obtain sufficient information for statistically acceptable results to reduce the number of experimental sets, and is an efficient method to evaluate the effects of multiple parameters, alone or in combination, on response variables.

3. Results and Discussion

3.1 Mechanical Properties

3.1.1 Flexural Strength. Figure 1 illustrates the impacts of dopant and sintering temperature upon 3Y-TZP flexural strength. Fluctuation in the flexural strength for the samples was noted between 320 and 600 MPa for a low temperature of sintering: 1250 °C. Nonetheless, upon sintering that exceeds 1350 °C, the strength of the doped 3Y-TZP began to improve, especially for samples that contained 0.3 wt.% Al_2O_3/0.5 wt.% CeO_2 and 0.3 wt.% Al_2O_3/0.3 wt.% CeO_2, which appeared to
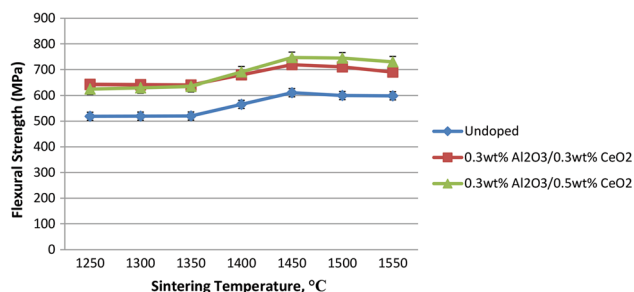
Fig. 1 Influence of CeO_2 and Al_2O_3 additions and sintering temperature on the flexural strength of 3Y-TZP
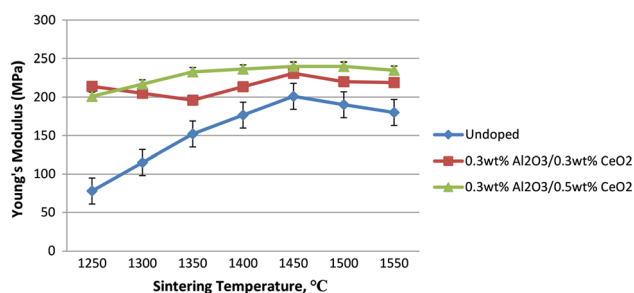
Fig. 2 Variations in Young's modulus for 3Y-TZP sintered samples in the range of 1250-1450 °C

be the best two compositions among the rest based on the outcomes. In particular, the 3Y-TZP sample consisting of 0.3 wt.% Al_2O_3/0.5 wt.% CeO_2 recorded the highest strength value, which increased from $\sim$ 638 MPa at 1350 °C to $\sim$ 750 MPa at 1450 °C.

Generally, the flexural strength of all doped 3Y-TZP samples increased compared to the undoped samples. One possible factor contributing to the high flexural strength of 0.3 wt.% Al_2O_3-0.5 wt.% CeO_2-doped 3Y-TZP could be associated with the tetragonal stability in the zirconia matrix. The result is in agreement with the findings of Matsui et al. (Ref 17) and Hiroshi et al. (Ref 18). The authors managed to attain strength values of 980 and 1200 MPa, respectively, and stated that the cause for high bending strength is also associated with fine ZrO_2 grains, low porosity, and yttria content.

3.1.2 Young's Modulus. Figure 2 displays the variations of Young's modulus (E) for 3Y-TZP with varied sintering temperatures and concentrations of dopant. It was observed that inclusion of $\geq$ 0.6 wt.% CeO_2 and Al_2O_3 had been exceptional to improve zirconia matrix stiffness upon sintering at a range of temperature 1250-1450 °C. For example, the values of E for > 130 GPa had been determined for samples that contained $\geq$ 0.6 wt.% CeO_2 and Al_2O_3, in comparison with undoped samples at 78 GPa sintered at 1250 °C. As such, 3Y-TZP that was undoped required higher temperature for sintering: 1350 °C, in order to obtain the E value of 150 GPa. However, sintering that exceeded 1350 °C caused a minor hike in the E value, while 195 GPa at its maximum for that 3Y-TZP undoped and sintered at a temperature of 1450 °C.

Nevertheless, when the sintering temperature exceeded 1450 °C, all the samples displayed a reduction in their values of E. This finding is in line with the reduction noted in the density of bulk as well as an increment in the content of cubic phase as the temperature was increased. With that, upon correlating the values of E with sintered density of bulk, a linear correlation was obtained. In fact, the value of E for the sintered 3Y-TZP seemed to increase in a linear manner up to a maximum of > 210 GPa as the density of bulk increased up to > 5.85 Mgm^{-3} regardless of the presence of dopant.

Hence, density of bulk is an essential parameter that determines the stiffness matrix of 3Y-TZP. Nonetheless, when the sintering temperature exceeded 1450 °C, all E values for the samples decreased. This scenario is in line with that depicted by Ramesh et al. (Ref 19), whereby the reduction in density of bulk is associated with grain growth due to the increment in temperature for sintering.

3.2 Tribological Properties

Tribological experiments were carried out on the 0.3 wt.% Al_2O_3/0.5 wt.% CeO_2 and 0.3 wt.% Al_2O_3/0.3 wt.% CeO_2-doped 3Y-TZP samples in an environment containing Ringer's solution. The experiments were conducted with disks and pins in three loading conditions: 10, 30, and 50 N. A comparison between the coefficients of friction (COF) of the best 3Y-TZP samples and loading conditions is presented in Fig. 3(a), (b), and (c), respectively. For each loading condition (10, 30, and 50 N), the 0.3 wt.% Al_2O_3/0.5 wt.% CeO_2 3Y-TZP samples generated lower friction coefficients (0.21, 0.325, and 0.407, respectively) than the 0.3 wt.% Al_2O_3/0.3 wt.% CeO_2-doped 3Y-TZP samples. According to the results, the properties of the counter materials affected the friction and wear characteristics of the materials.
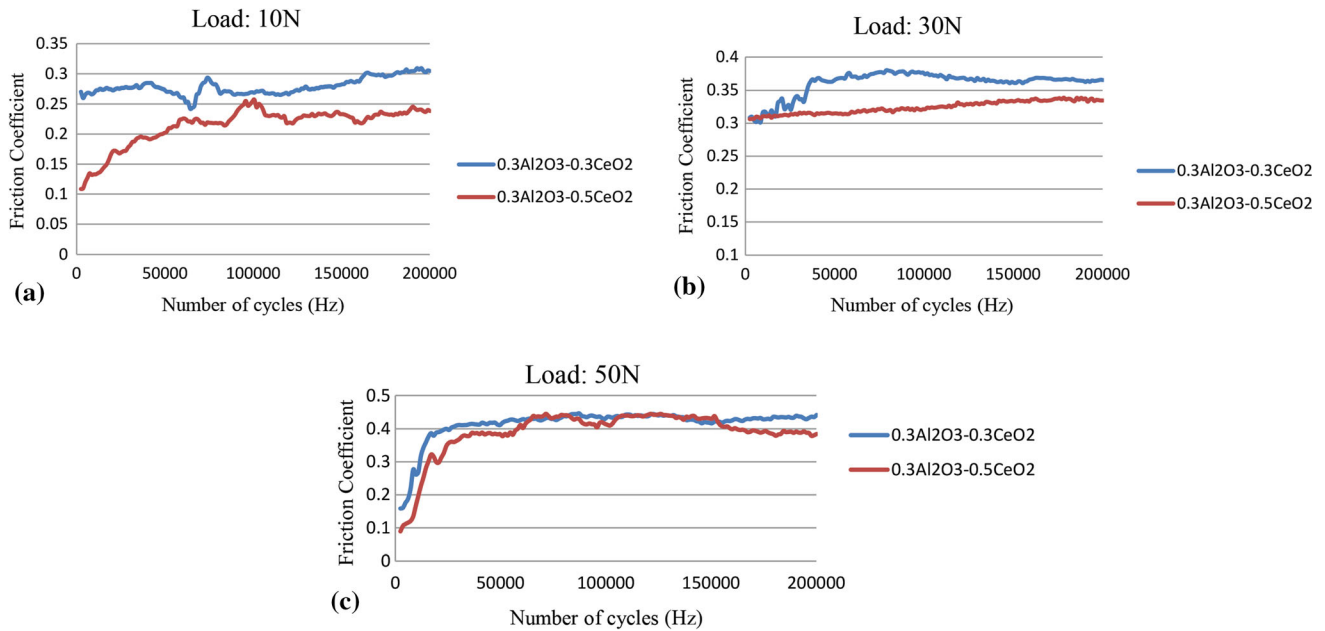
Fig. 3 Friction coefficient profiles for: (a) 10 N, (b) 30 N, and (c) 50 N
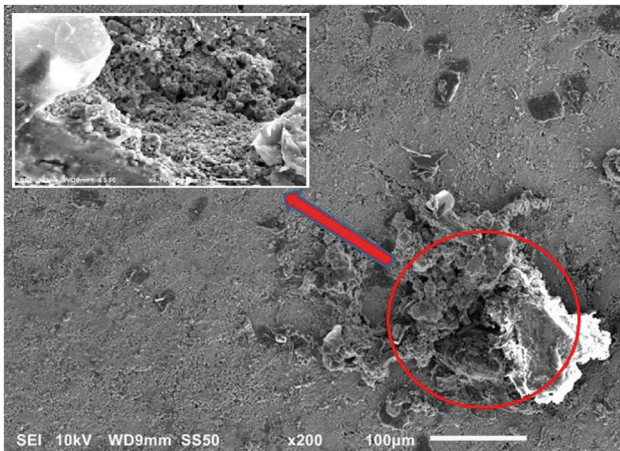
Fig. 4 Surface area of the 0.3 wt.% Al_2O_3/0.3 wt.% CeO_2 samples after wear

Fig. 5 Variations of specific wear rate with different applied loads for various compositions

The coefficient of friction (COF) for 0.3 wt.% Al_2O_3/0.3 wt.% CeO_2-doped 3Y-TZP samples was slightly higher than that for 0.3 wt.% Al_2O_3/0.5 wt.% CeO_2, and it apparently increased slightly with load ($\sim$ 0.25-0.45). This result is considerably superior to the wear properties of pure Y-TZP, whereby the COF of Y-TZP varied between 0.45 and 0.7, depending on speed and load combination. Suh et al. (Ref 20) reported the wear rate of the ZrO_2/ZrO_2 pair was 5.04×10^{-4} mm^3/Nm, which is in good agreement with the current result. For the loads of 10 and 30 N, the COF increased with the increase in the number of cycles (Hz), whereas for the 50 N load, the COF increased drastically to a high value at the beginning (4000-8000 cycles) and subsequently attained a steady-state value. The data in Fig. 3 indicate that the average COF for all 3 loads ranged from 0.4 to 0.5.

Figure 4 illustrates the 0.3 wt.% Al_2O_3/0.3 wt.% CeO_2 hydrothermally loaded 3Y-TZP surfaces after cyclic loading

under ambient air conditions immersed in Ringer solution. The surface damage in the micro-slip zone is obvious in Fig. 4. It can be clearly observed that minor fretting incidences are generated within the micro-slip zone. They are unevenly distributed and vary in size and shape. Surface fatigue in terms of local micro-fracture can be observed in addition to dark-colored debris particles from the CeO_2 sphere which are located in adjacency to fretting scars. The surface fatigue is highly pronounced in this area, and surface macro-cracking is clearly visible. It is also evident that the surface grains are uplifted at local spots, and as a consequence, the pull-out of grains has occurred.

The highest wear rate (4.12×10^{-4} mm^3/Nm) was observed for 3Y-TZP samples containing 0.3 wt.% Al_2O_3/0.3 wt.% CeO_2 when subjected to the 50 N loads, as seen in Fig. 5. Figure 6 presents the surface roughness of 3Y-TZP samples before and after wear as well as after exposure to 100 h of aging. The results reveal that the surface roughness was significantly higher for pure 3Y-TZP (Ra = 0.49) than for the Al_2O_3- and CeO_2-doped 3Y-TZP samples (Ra = 0.42).

3.3 Degradation Properties

A huge drawback of 3Y-TZP ceramics refers to the conversion from (t) to (m) symmetry as well as degradation of the property at the exposure to humidity. In this study, two methods were used to identify the degradation: (i) accelerated aging performed in an autoclave (aging bomb) and (ii) immersion of selected 3Y-TZP samples in Ringer's solution. With the first method, selected sintered 3Y-TZP samples were exposed to superheated steam at 134 °C, or 2 bars in the autoclave for the durations ranging from 0 to 100 h. The monoclinic phase content of each 3Y-TZP sample was monitored at selected intervals during the hydrothermal treatment to determine the extent of the aging-induced phase transformation that occurred. With the second method, fourteen sintered 3Y-TZP samples were selected from the two best compositions (0.3 wt.% Al_2O_3/0.5 wt.% CeO_2 and 0.3 wt.% Al_2O_3/0.3 wt.% CeO_2) and exposed to Ringer's solution at room temperature in a vacuum environment for 1-6 months. Furthermore, two methods were used to identify the presence of 3Y-TZP sample degradation: (i) 3Y-TZP sample weight loss and (ii) SEM to determine the formation of a porous structure and grain size increase.

3.3.1 Phase Stability and Aging Behavior. A such, the feature of aging for undoped, 0.3 wt.% Al_2O_3/0.3 wt.% CeO_2 and 0.3 wt.% Al_2O_3/0.5 wt.% CeO_2-doped 3Y-TZPs had been investigated via XRD so as to evaluate the quantity of monoclinic phase content at the surface of the samples due to conversion from tetragonal to monoclinic with varied aging intervals. Next, Table 2 and Fig. 7 display the quantity of surface monoclinic content among the samples, which were sintered at 1450 °C, after being exposed for 100 h to steam that was superheated. As a result, samples that were undoped
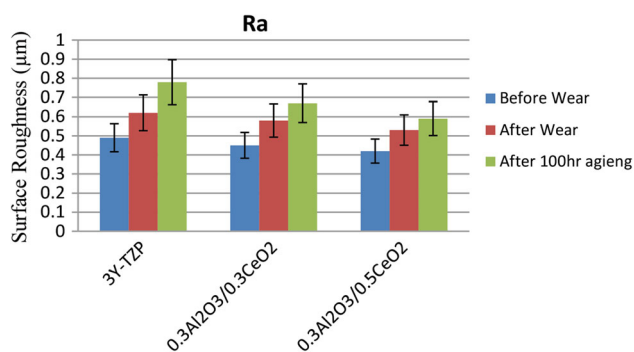
appeared to be the worst types as they displayed 80% conversion only after an hour of aging. Besides, more than 95% of the tetragonal microstructure surface appeared to have transformed to monoclinic after 3-h exposure. Furthermore, the 0.3 wt.% Al_2O_3/0.5 wt.% CeO_2 sample showed the best resistance for aging with 36% conversion after 100 h of aging.

The material loss shown in Fig. 8 occurred throughout the aging process for undoped Y-TZP that exhibited severe phase transformation. These observations strongly testify to a phenomenon of LTD transformation commonly reported by other researchers, whereby aging proceeds from the material's surface to its interior (Ref 21, 22). However, the 0.3 wt.% Al_2O_3/0.5 wt.% CeO_2 and 0.3 wt.% Al_2O_3/0.3 wt.% CeO_2-doped 3Y-TZP samples exhibited minimal weight loss up to 100 h. The overall weight loss in this study is slightly higher (0.004 g) than the weight loss of the Y-TZP ball head observed by Heimann (Ref 23), which was only 0.002 g. The authors conducted a corrosion test on a Y-TZP femoral ball head by immersing it in Ringer's solution at 37 °C and pH 7 and observing it for up to 800 days. In the current research, the maximum weight loss observed was 0.004 and 0.008 g. The greater weight loss is probably attributed to the preparation technique, the presence of impurities as well as the sintering temperature. The higher sintering temperature (i.e., > 1450 °C) could have caused a slight increase in zirconia grain size (attributed to grain growth), making the material more susceptible to degradation.

3.3.2 Weight Loss Measurement. The additions of 0.3 wt.% Al_2O_3/0.5 wt.% CeO_2 and 0.3 wt.% Al_2O_3/0.3 wt.% CeO_2 appeared to be the best compositions for achieving superior mechanical properties. The aging behavior

Fig. 6 Surface roughness values (Ra) before wear, after wear and after 100-h aging for different material compositions
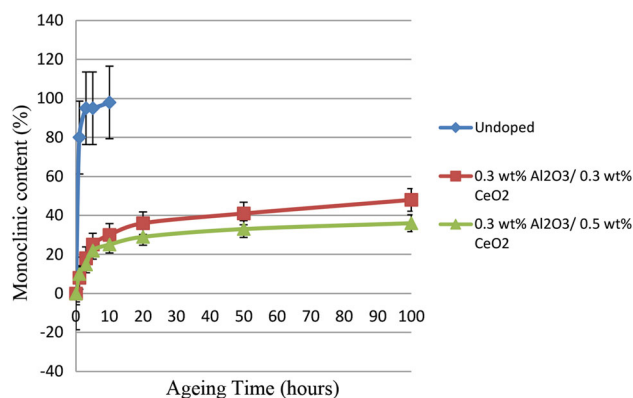
Fig. 7 Amounts of surface monoclinic content generated at different intervals up to 100 h of aging for all 3Y-TZPs sintered at 1450 °C

Table 2 Monoclinic content and grain size of 0.3 wt.% Al_2O_3/0.3 wt.% CeO_2 and 0.3 wt.% Al_2O_3/0.5 wt.% CeO_2 degraded in superheated steam

Specimens	Grain size, μm	Monoclinic content, %	Aging time, h
Undoped	1.23 ± 0.05	> 95	3
0.3 wt.% Al_2O_3/0.3 wt.% CeO_2	0.545 ± 0.005	± 50	100
0.3 wt.% Al_2O_3/0.5 wt.% CeO_2	0.422 ± 0.005	± 36	100
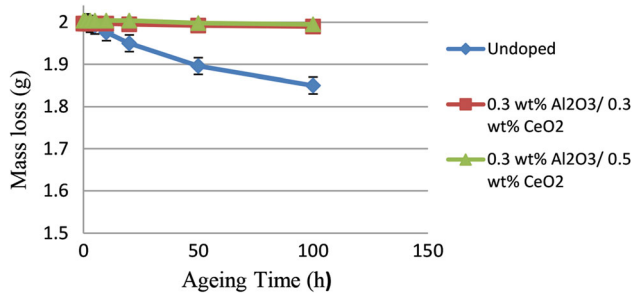
Fig. 8 Mass loss of Y-TZP samples sintered at 1450 °C as a function of aging time
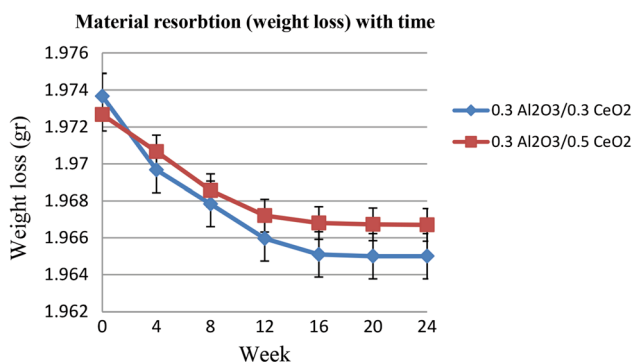
Fig. 9 Weight loss comparison for the 0.3 wt.% Al_2O_3/0.3 wt.% CeO_2 and 0.3 wt.% Al_2O_3/0.5 wt.% CeO_2 samples over 24 weeks

of these 3Y-TZP samples was observed over 0, 4, 8, 12, 16, 20, and 24 weeks. The weights of the 3Y-TZP samples were recorded each week to measure the weight loss that occurred during the immersion period. Two sets of 3Y-TZP samples, Set A and Set B were used to obtain the average weight loss each week. The results indicated the degradation of 3Y-TZP samples. As seen in Fig. 9, there was a marginal decrease in weight as the time period increased. When comparing the 3Y-TZP samples, it was observed that the weight loss of the 3Y-TZP sample containing 0.3 wt.% Al_2O_3/0.3 wt.% CeO_2 was 0.0088 g, while the 3Y-TZP sample containing 0.3 wt.% Al_2O_3/0.5 wt.% CeO_2 recorded weight loss of 0.0061 g at the end of week 24.

Apart from the tetragonal to monoclinic phase transformation, the 3Y-TZP samples undergoing the LTD process were accompanied by structural and property deterioration. When the aging duration was prolonged, a considerable reduction in 3Y-TZP sample bulk density and weight (weight loss due to surface spalling) was measured, as shown in Table 3 and Fig. 9, respectively. This deterioration is consistent with the fundamental characteristics of LTD, as reported by many researchers (Ref 24-26).

The variations in bulk density before and after aging for 100 h are shown in Table 3. It was found that the addition of dopants to 3Y-TZP was effective in maintaining the tetragonal grain stability of the sintered body (1450 °C) without sacrificing bulk density. The bulk density after 100 h for the 3Y-TZP sample containing 0.3 wt.% Al_2O_3/0.5 wt.% CeO_2 reduced by only 0.12%, while for the undoped 3Y-TZP sample the reduction rate was 2.7%.

3.3.3 Microstructural Analysis. The second method used to identify the presence of degradation in the doped 3Y-TZP samples is explained in this section. At each interval (i.e., 0, 4, 8, 12, 16, 20, and 24 weeks), the 3Y-TZP samples underwent scanning electron microscopy (SEM) imaging to analyze whether porous structures formed and the grain size increased. The SEM images of the 3Y-TZP samples containing 0.3 wt.% Al_2O_3/0.3 wt.% CeO_2 immersed in Ringer's solution in sequence from the initial week (week 0) up until the final week (week 24) are shown in Fig. 10. It is observed that the grain size increased for every 3Y-TZP sample as the immersion period increased. The initial grain and pore sizes at week 0 were 0.431 and 0.829 μm, respectively, while the final grain and pore sizes recorded were 0.560 and 1.289 μm, respectively, at week 24. The initial and final grain sizes showed a difference of 23%, while the pore sizes displayed a difference of 36%. The results showed that the weight loss experienced by the samples had been linearly proportional to the increment in size of grain. As such, it is verified that a number of parameters, for instance, methods of processing the powder, compositions that include dopants and yttria, and sintering temperatures, as well as microstructural features, for example, size of grain and grain boundary phase presence, seemed to be significant to determine the behavior of aging for 3Y-TZP ceramic.

In a similar manner, the SEM images of samples that contained 0.3 wt.% Al_2O_3/0.5 wt.% CeO_2 and immersed in a solution of Ringer are illustrated in Fig. 11, based on the arrangement from the first week (week 0) until the last (week 24). Furthermore, the samples' pore size and grain of the 0.3 wt.% Al_2O_3/0.5 wt.% CeO_2-doped 3Y-TZP had been determined. The initial grain and pore sizes recorded at week 0 were 0.388 and 0.559 μm, respectively, whereas the final grain and pore sizes recorded at week 24 were 0.513 and 1.154 μm, respectively. The difference in grain size was 24%, while the difference in pore size was 51%. It is also observed that both grain and pore sizes increased for every 3Y-TZP sample as the immersion period increased. Figure 10 indicates that 3Y-TZP sample weight loss is linearly proportional to the increase in 3Y-TZP sample grain size. When comparing the 3Y-TZP samples containing 0.3 wt.% Al_2O_3/0.3 wt.% CeO_2 and 0.3 wt.% Al_2O_3/0.5 wt.% CeO_2, it is evident that the former had larger grain and pore sizes at the end of week 24.

4. Conclusions

With a suitable composition, alumina-ceria-3Y-TZP bioceramic appears to be a promising bioceramic that provides low wear rate. The dopant composition of 0.3 wt.% Al_2O_3 and 0.5 wt.% CeO_2 was found to be the optimal that demonstrated lower coefficient of friction (COF) along with superior mechanical properties compared to other compositions. The aging investigation results showed the minimal effect of aging on the 0.3 wt.% Al_2O_3/0.5 wt.% CeO_2-doped 3Y-TZP samples. Furthermore, accelerated aging in an autoclave up to 100 h further validated the findings, while the 0.3 wt.% Al_2O_3/0.5 wt.% CeO_2 produced a minimal degradation rate of 36%. Scanning electron microscopy (SEM) also revealed that 0.3 wt.% Al_2O_3/0.5 wt.% CeO_2 dopant composition produced smaller grain size than other compositions despite aging. The preliminary results suggest that the 0.3 wt.% Al_2O_3/0.5 wt.% CeO_2-doped 3Y-TZP bioceramic demonstrates great potential

Table 3 Bulk densities of 3Y-TZP (sintered at 1450 °C) before and after aging treatment

	Aging duration		
Al$_2$O$_3$/CeO$_2$ content, wt.%	0 h	100 h	% difference in bulk density
0 (Undoped)	5.890 (kg/m^3)	5.732 (kg/m^3)	2.7
0.3Al$_2$O$_3$/0.3CeO$_2$	5.956 (kg/m^3)	5.907 (kg/m^3)	0.82
0.3Al$_2$O$_3$/0.5CeO$_2$	5.955 (kg/m^3)	5.948 (kg/m^3)	0.12

(a) (b)
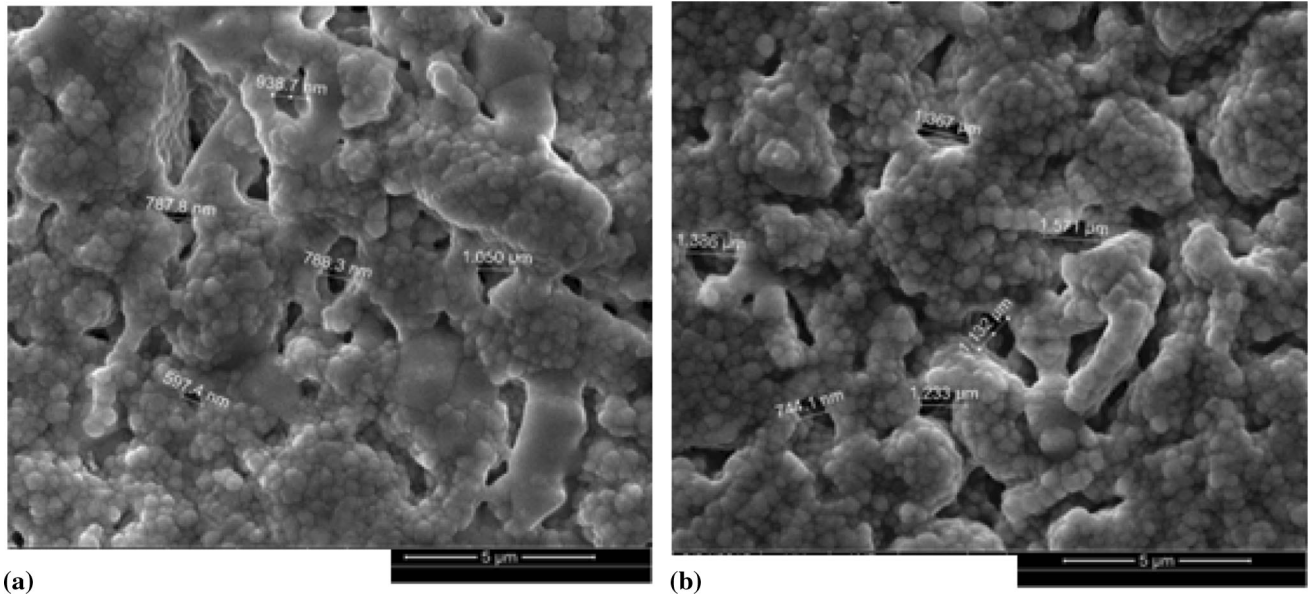
Fig. 10 SEM images of the porous structures of 3Y-TZP samples doped with 0.3 wt.% Al$_2$O$_3$ and 0.3 wt.% CeO$_2$: (a) degradation period of 0 week and (b) 24 weeks

(a) (b)
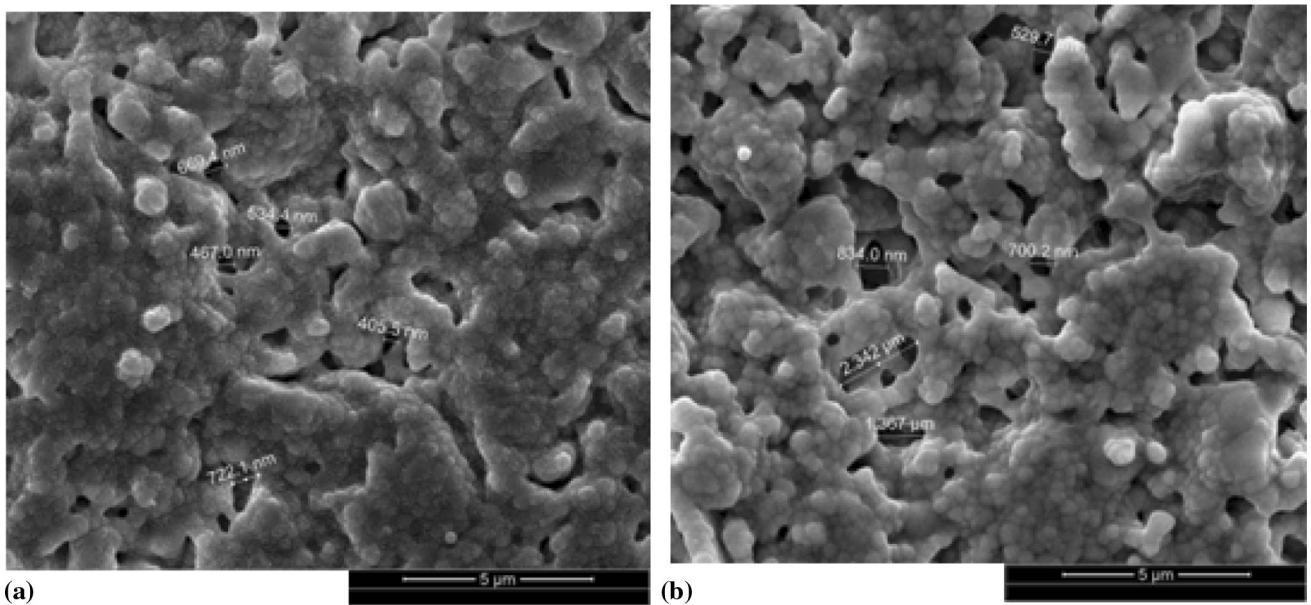
Fig. 11 SEM images displaying the porous structures of samples containing 0.3 wt.% Al$_2$O$_3$/0.5 wt.% CeO$_2$ at (a) week 0 and (b) week 24

for biomedical implant applications seemingly due to its optimal set of properties. However, it mandates further in-depth investigations for a viable conclusion.

Conflict of interest

The authors declare that there is no conflict of interests regarding the publication of this paper.

References

1. B. Bikramjit, J. Vleugels, and O. Van der Biest, Microstructure–Toughness–Wear Relationship of Tetragonal Zirconia Ceramics, *J. Eur. Ceram. Soc.*, 2004, **24**, p 2031–2040
2. C. Aksel, Mechanical Properties and Thermal Shock Behaviour of Alumina-Mullite-Zirconia and Alumina-Mullite Refractory Materials by Slip Casting, *Ceram. Int.*, 2003, **29**, p 311–316
3. G.Y. Akimov and V.M. Timchenko, Mechanical Properties of Ceramics Prepared from a Nanocrystalline ZrO_2-3 mol.% Y_2O_3 Powder, *Refract. Ind. Ceram.*, 2004, **45**, p 55–57
4. S. Ramesh, C. Gill, S. Lawson, and G.P. Dransfield, The Effect of Copper Oxide on Sintering, Microstructure, Mechanical Properties and Hydrothermal Ageing of Coated 2.5Y-TZP Ceramics, *J. Mater. Sci.*, 1999, **34**, p 5457–5467
5. B. Bikramjit, J. Vleugels, and O. Van der Biest, Toughness Tailoring of Yttria-Doped Zirconia Ceramics, *Mater. Sci. Eng. A*, 2004, **380**, p 215–221
6. W. Dworak and D. Fingerle, Ceramics Materials for Engines, *Ceram. Trans. J.*, 1987, **86**, p 170–182
7. A.M. Anthony, Effect of Sintering Temperature on Mechanical Properties of Magnesia Partially Stabilized Zirconia Refractory, *Ceram. Int.*, 2016, **42**, p 10593–10598
8. N. Claussen, Strengthening Strategies For ZrO_2-Toughened Ceramics at High Temperatures, *Mater. Sci. Eng.*, 1985, **71**, p 23–38
9. M. Golieskardi, M. Satgunam, D. Ragurajan, and M.N.M. Ansari, The Effect of Aluminum Oxide (Al_2O_3) and Cerium Oxide (CeO_2) on the Structural and Mechanical Properties of Yttria Tetragonal Zirconia Polycrystal (Y-TZP), *J. Aust. Ceram. Soc.*, 2015, **51**, p 16–21
10. J.R. Seidensticker and M.J. Mayo, Superplasticity in 3Y-TZP Doped with Small Amounts of Copper Oxide, *Scr. Metall. Mater.*, 1994, **31**, p 1749–1754
11. M. Guazzatoa, M. Albakrya, S.P. Ringerb, and M.V. Swaina, Strength, Fracture Toughness and Microstructure of a Selection of All-Ceramic Materials. Part I. Pressable and Alumina Glass-Infiltrated Ceramics, *Dent. Mater.*, 2004, **20**, p 441–448
12. S. Lawson, Review—Environmental Degradation of Zirconia Ceramics, *J. Eur. Ceram. Soc.*, 1995, **15**, p 485–502
13. G.K.R. Pereira, A.B. Venturini, T. Silvestri, K.S. Dapieve, A.F. Montagner, F.Z.M. Soares, and L.F. Valandro, Low-Temperature Degradation of Y-TZP Ceramics: A Systematic Review and Meta-analysis, *J. Mech. Behav. Biomed. Mater.*, 2016, **55**, p 151–163
14. X. Guo, Hydrothermal Degradation Mechanism of Tetragonal Zirconia, *J. Mater. Sci.*, 2001, **36**, p 3737–3744
15. S.M. Kurtz, S. Kocagöz, C. Arnholt, R. Huet, M. Ueno, and W.L. Walter, Advances in Zirconia Toughened Alumina Biomaterials for Total Joint Replacement, *J. Mech. Behav. Biomed. Mater.*, 2014, **31**, p 107–116
16. C.J. Howard and R.J. Hill, The Polymorphs of Zirconia: Phase Abundance and Crystal Structure by Rietveld Analysis of Neutron and x-ray Diffraction Data, *J. Mater. Sci.*, 1991, **26**, p 127–134
17. K. Matsui, H. Yoshida, and Y. Ikuhara, Grain-Boundary Structure and Microstructure Development Mechanism in 2-8 mol.% Yttria-Stabilized Zirconia Polycrystals, *Acta Mater.*, 2008, **56**, p 1315–1325
18. O. Hiroshi, N. Hironori, S. Tohru, I. Yuichi, and N. Koichi, Mechanical Properties of 2.0-3.5 mol.% Y_2O_3-Stabilized Zirconia Polycrystals Fabricated by the Solid Phase Mixing and Sintering Method, *J. Ceram. Soc. Jpn.*, 2008, **12**, p 1270–1277
19. S. Ramesh, S. Meenaloshini, C.Y. Tan, W.J. Kelvin Chew, and W.D. Teng, Effect of Manganese Oxide on the Sintered Properties and Low Temperature Degradation of Y-TZP Ceramics, *Ceram. Int.*, 2008, **34**, p 1603–1608
20. M.S. Suh, Y.H. Chae, and S.S. Kim, Friction and Wear Behavior of Structural Ceramics Sliding Against Zirconia, *Wear*, 2008, **264**, p 800–806
21. E. Lilley, Review of Low Temperature Degradation of Tetragonal Zirconia Ceramics, *Ceramics Transactions, Corrosion and Corrosive Degradation of Ceramics*, Vol 10, R.E. Tressler and H. McNallen, Ed., American Ceramic Society, Westerville, 1990, p 387–406
22. J. Chevalier, L. Gremillard, and S. Deville, Low-Temperature Degradation of Zirconia and Implications for Biomedical Implants, *Annu. Rev. Mater. Res.*, 2007, **37**, p 1–32
23. R.B. Heimann, Materials Science of Crystalline Bioceramics: A Review of Basic Properties and Applications, *CMU J.*, 2002, **1**, p 23–45
24. P. Kanellopoulos and C. Gill, Hydrothermal Ageing of Yttria-Stabilized Zirconia, Sintered at 1300-1325 °C: The Effects of Copper Oxide Doping and Sintering Time Variations, *J. Mater. Sci.*, 2002, **37**, p 5075–5082
25. F. Kern and R. Gadow, Mechanical Properties and Low Temperature Degradation Resistance of 2.5Y-TZP-Alumina Composites, *Mater. Ceram.*, 2013, **65**, p 258–266
26. S.M. Kw, S. Ramesh, L.T. Bang, Y.H. Wonga, W.J. Kelvin Chew, C.Y. Tan, J. Purbolaksono, H. Misran, and W.D. Teng, Effect of Sintering Holding Time on the Properties and Low-Temperature Degradation Behaviour of Manganese Oxide-Doped Y-TZP Ceramic, *J. Ceram. Process. Res.*, 2015, **16**, p 193–198